Inhibition of the UFD-1-NPL-4 complex triggers an inflammation-like response in *Caenorhabditis elegans*

Rajneesh Rao[1] , Alejandro Aballay[2], and Jogender Singh[1,*]

[1]Department of Biological Sciences, Indian Institute of Science Education and Research, Mohali, Punjab, 140306, India

[2]Department of Molecular Microbiology & Immunology, Oregon Health & Science University, Portland, OR 97239, USA

[*]For correspondence: jogender@iisermohali.ac.in

Keywords: Colonization, ERAD, GATA transcription factor, inflammation, ubiquitin-proteasome system

Abstract

The UFD-1 (ubiquitin fusion degradation 1)-NPL-4 (nuclear protein localization homolog 4) heterodimer is involved in extracting ubiquitinated proteins from several plasma membrane locations, including the endoplasmic reticulum. This heterodimer complex helps in the degradation of ubiquitinated proteins via proteasome with the help of AAA+ ATPase CDC-48. While the ubiquitin-proteasome system is known to have important roles in maintaining innate immune responses, the role of the UFD-1-NPL-4 complex in regulating immunity remains elusive. In this study, we investigate the role of the UFD-1-NPL-4 complex in maintaining *Caenorhabditis elegans* innate immune responses. Inhibition of the UFD-1-NPL-4 complex activates an inflammation-like response that reduces the survival of the wild-type worms on the pathogenic bacterium *Pseudomonas aeruginosa* despite diminishing colonization of the gut with the bacterium. This inflammation-like response improves the survival of severely immunocompromised worms on pathogenic bacteria but is detrimental on nonpathogenic bacteria. Transcriptomics studies reveal that the GATA transcription factor ELT-2 mediates the inflammation-like response upon inhibition of the UFD-1-NPL-4 complex. Our studies uncover important roles of the UFD-1-NPL-4 complex in innate immunity and reveal the existence of inflammation-like responses in *C. elegans*.

Introduction

Maintenance of a healthy proteome involves the degradation of misfolded proteins (Vembar and Brodsky, 2008; Vilchez et al., 2014). Proteasomes are a major site for the degradation of misfolded proteins (Clague and Urbe, 2010; Ding and Yin, 2008). Proteins are tagged for proteasomal degradation by ubiquitin through a series of enzymatic reactions (Dikic, 2017). In addition to the proteasomal degradation of proteins, ubiquitination controls a vast array of cellular signals and functions (Husnjak and Dikic, 2012; Mukhopadhyay and Riezman, 2007). The ubiquitination pathways also have important roles in innate immunity regulation (Garcia-Sanchez et al., 2021; Li et al., 2016). The host ubiquitination pathways are involved in the targeting of bacterial proteins, lipopolysaccharides, and bacteria-containing vacuoles, resulting in selective macroautophagy or xenophagy of bacterial pathogens (Chai et al., 2019; Haldar et al., 2015; Otten et al., 2021; Tripathi-Giesgen et al., 2021). Because of the important roles of ubiquitination in host defenses, bacterial pathogens have evolved multiple strategies to target the host ubiquitination pathways (Bomberger et al., 2011; Herhaus and Dikic, 2018; Ribet and Cossart, 2018). Therefore, it is possible that inhibition of the ubiquitination pathways would activate immune responses via compensatory mechanisms.

The proteasomal degradation requires ubiquitin-tagged proteins to be unfolded and extracted from macromolecular complexes (Boom and Meyer, 2018). CDC-48 (VCP/p97 in vertebrates) is a highly conserved AAA+ ATPase that uses its protein unfoldase activity to extract a variety of ubiquitinated polypeptides from membranes or macromolecular complexes (Bodnar and Rapoport, 2017; Meyer et al., 2012). CDC-48 uses different cofactor proteins to recognize its client proteins (Meyer et al., 2012). The UFD-1 (ubiquitin fusion degradation 1)-NPL-4 (nuclear protein localization homolog 4) heterodimer is a CDC-48 cofactor that is involved in the extraction of misfolded and ubiquitinated proteins from several plasma membrane locations, including the endoplasmic reticulum (ER) (Meyer et al., 2000; Wolf and Stolz, 2012; Ye et al., 2001). Therefore, the UFD-1-NPL-4 complex is critical for the ER-associated degradation (ERAD) of misfolded proteins (Wu and Rapoport, 2018). In addition to ERAD, the ER has evolved other strategies to deal with misfolded proteins (Singh, 2023), including a series of unfolded protein response (UPR) pathways that enhance the folding capacity of the ER by synthesis of molecular chaperones and reduction of protein translation (Hetz et al., 2015). The ER-UPR pathways are required for an optimum immune response (Engel and Barton, 2010; Richardson et al., 2010; Sun et al., 2012). However, the role of the UFD-1-NPL-4 complex, which is required for ERAD, in regulating immune responses remains poorly explored. Because ubiquitin-dependent pathways have important roles in immunity, it will be interesting to explore the role of the UFD-1-NPL-4 complex in regulating immune responses.

In this study, we showed that the inhibition of the UFD-1-NPL-4 complex results in the activation of an inflammation-like response in *Caenorhabditis elegans*. The wild-type worms had a drastic reduction in survival on the pathogenic bacterium *Pseudomonas aeruginosa* despite having diminished colonization of the gut with the bacterium. Inhibition of the UFD-1-NPL-4 complex also led to diminished bacterial colonization in mutants of ER-UPR and immunity pathways. The diminished bacterial colonization improved the survival of severely immunocompromised mutants on pathogenic bacteria. However, on nonpathogenic bacteria, on which the severely immunocompromised mutants exhibit a normal lifespan, inhibition of the UFD-1-NPL-4 complex resulted in a drastic reduction in lifespan. Transcriptomic studies revealed that inhibition of the UFD-1-NPL-4 complex resulted in the activation of the intracellular pathogen response. Analysis for transcription factor enrichment for upregulated genes identified that the GATA transcription factor ELT-2 mediated the inflammation-like response upon inhibition of the UFD-1-NPL-4 complex. Our studies

uncovered important roles of the UFD-1-NPL-4 complex in innate immunity and revealed the existence of inflammation-like responses in *C. elegans*.

Results

Inhibition of the UFD-1-NPL-4 complex reduces survival of *C. elegans* on *P. aeruginosa*

To explore the role of the UFD-1-NPL-4 complex in the innate immune response of *C. elegans*, we knocked down *ufd-1* and *npl-4* by RNA interference (RNAi) and studied the survival of the worms on the pathogenic bacterium *P. aeruginosa* PA14. Knockdown of *ufd-1* and *npl-4* resulted in a drastic reduction in the survival of N2 wild-type worms on *P. aeruginosa* compared to worms grown on control RNAi (Figure 1A). The animals also had a reduced lifespan on *Escherichia coli* HT115 upon knockdown of *ufd-1* and *npl-4* (Figure 1B). The relationship between *C. elegans* innate immunity and longevity pathways is complex. Mutants that have reduced lifespan but improved immunity have been identified (Amrit et al., 2019; Otarigho and Aballay, 2021; Ren and Ambros, 2015). Moreover, immunocompromised animals such as mutants of the MAP kinase pathway mediated by NSY-1/SEK-1/PMK-1 have a normal lifespan despite having drastically reduced survival on pathogenic bacteria (Kim et al., 2002; Liberati et al., 2004). Therefore, we explored the mechanisms that led to the reduced survival of *ufd-1* and *npl-4* knockdown animals on *P. aeruginosa*. Colonization of the gut with *P. aeruginosa* is a major determinant of infection and survival of *C. elegans* under slow-killing conditions (Das et al., 2023; Tan et al., 1999). Because knockdown of *ufd-1* and *npl-4* reduced survival on *P. aeruginosa*, we asked whether the animals had enhanced colonization of the gut with *P. aeruginosa* after *ufd-1* and *npl-4* RNAi. Surprisingly, we observed that *ufd-1* and *npl-4* knockdown resulted in reduced colonization of the gut with *P. aeruginosa* (Figure 1C and 1D). To validate further, we performed the colony-forming unit assay (CFU) upon knockdown of *ufd-1* and *npl-4*. There was a significant decline in the CFU per worm in *ufd-1* and *npl-4* knockdown worms, indicating reduced numbers of live bacteria in these worms (Figure 1E).

Reduced colonization of the gut by *P. aeruginosa* could be because of reduced uptake of the bacterium in *ufd-1* and *npl-4* knockdown animals. The rate of pharyngeal pumping is an indicator of the uptake of bacterial food. We studied whether inhibition of *ufd-1* and *npl-4* affected the pharyngeal pumping rate. The knockdown of *ufd-1* and *npl-4* did not affect the pharyngeal pumping rate (Figure S1A), indicating that the reduced colonization was unlikely due to the reduced uptake of bacteria. Next, we tested whether exposure to *P. aeruginosa* affected the pharyngeal pumping in *ufd-1* and *npl-4* knockdown animals. Exposure to *P.*

aeruginosa for 12 hours resulted in a minimal reduction in the pharyngeal pumping rate in *ufd-1* and *npl-4* knockdown animals compared to control animals (Figure S1B). These results suggested that the reduced colonization of *ufd-1* and *npl-4* knockdown animals by *P. aeruginosa* was unlikely because of the reduced uptake of bacteria. Taken together, these results suggested that the inhibition of the UFD-1-NPL-4 complex reduced the survival of *C. elegans* on *P. aeruginosa* despite diminished colonization of the gut with the bacterium. Because *ufd-1* and *npl-4* RNAi led to very similar phenotypes, we further used only *ufd-1* RNAi to decipher the mechanisms of reduced survival and diminished colonization on *P. aeruginosa*.

Reduced colonization with *P. aeruginosa* upon *ufd-1* knockdown is independent of the ER-UPR pathways

Knockdown of the UFD-1-NPL-4 complex is known to cause ER stress, resulting in the upregulation of the ER-UPR pathways (Mouysset et al., 2006; Sasagawa et al., 2007). Because ER stress and UPR pathways modulate innate immunity (Richardson et al., 2010; Singh and Aballay, 2017; Sun et al., 2012), we asked whether the ER-UPR pathways were involved in the regulation of survival and colonization of *ufd-1* knockdown animals on *P. aeruginosa*. We studied the survival and colonization of mutants of different ER-UPR pathways, including *xbp-1(tm2482)*, *atf-6(ok551)*, and *pek-1(ok275)* on *P. aeruginosa*. The survival of *xbp-1(tm2482)* animals upon *ufd-1* knockdown was indistinct from the control animals (Figure 2A). However, *ufd-1* knockdown resulted in drastically reduced gut colonization with *P. aeruginosa* in *xbp-1(tm2482)* animals (Figure 2B and 2C). This indicated that the *xbp-1* pathway was not required for the reduced *P. aeruginosa* colonization of *ufd-1* knockdown animals.

The *atf-6(ok551)* animals exhibited reduced survival on *P. aeruginosa* upon *ufd-1* RNAi compared to the control RNAi (Figure 2D). Similar to N2, *ufd-1* knockdown resulted in reduced colonization of the gut with *P. aeruginosa* in *atf-6(ok551)* animals (Figure 2E and 2F). The *pek-1(ok275)* animals exhibited similar phenotypes of reduced survival and diminished colonization on *P. aeruginosa* upon *ufd-1* knockdown (Figure 2G-I). These results indicated that the reduced colonization and survival of *ufd-1* knockdown animals on *P. aeruginosa* were independent of the ER-UPR pathways.

Reduced colonization with *P. aeruginosa* upon *ufd-1* knockdown is independent of the major immunity pathways

Next, we tested whether any of the immunity pathways were involved in regulating the reduced colonization by *ufd-1* knockdown. To this end, we studied the survival and colonization of mutants of different immunity pathways on *P. aeruginosa* upon knockdown of *ufd-1*. The *pmk-1(km25)* animals, which are part of a MAP kinase pathway mediated by NSY-1/SEK-1/PMK-1 (Kim et al., 2002), had a similar survival rate on control and *ufd-1* RNAi (Figure 3A). However, *ufd-1* knockdown drastically reduced colonization in *pmk-1(km25)* animals (Figure 3B and 3C). This indicated that the *pmk-1* pathway is unlikely to be involved in mediating *ufd-1* knockdown effects, and the similar survival rate of control and *ufd-1* RNAi animals is merely coincidental. Indeed, a mutant of the upstream regulator of the PMK-1 pathway, the Toll/interleukin-1 receptor domain protein (TIR-1) (Liberati et al., 2004; Peterson et al., 2022), exhibited phenotypes similar to *pmk-1(km25)* animals (Figure S2A-C).

The mutants of the TGF-β/DBL-1 (Mallo et al., 2002) and TFEB/HLH-30 (Visvikis et al., 2014) immunity pathways also exhibited phenotypes similar to *pmk-1(km25)* animals. The knockdown of *ufd-1* resulted in drastically reduced colonization of *dbl-1(nk3)* and *hlh-30(tm1978)* animals without affecting their survival on *P. aeruginosa* (Figure 3D-I). These results indicated that the reduced colonization with *P. aeruginosa* upon *ufd-1* knockdown was independent of these immunity pathways.

Inhibition of the UFD-1-NPL-4 complex improves survival of severely immunocompromised *C. elegans* on *P. aeruginosa*

Knockdown of *ufd-1* reduced colonization in wild-type animals as well as mutants of ER-UPR and innate immunity pathways. Interestingly, despite variable survival rates on control RNAi, all strains had similar survival rates upon knockdown of *ufd-1* (Figure S3). We reasoned that *ufd-1* knockdown might lead to an inflammation-like response that results in diminished gut colonization by *P. aeruginosa* and reduces the survival of healthy but not immunocompromised animals. If the knockdown of the UFD-1-NPL-4 complex indeed resulted in an inflammation-like response, their knockdown should improve the survival of severely immunocompromised animals. In *C. elegans*, the canonical p38 MAP kinase signaling cascade consists of NSY-1 (ASK1 MAPKKK), SEK-1 (MKK3/MKK6 MAPKK), and PMK-1 (p38 MAPK) (Kim et al., 2002). Compared to *pmk-1* knockout, the knockout of *sek-1* leads to more severe effects on survival upon infection with *P. aeruginosa* (Meng et al., 2021). Indeed, we observed that most of the *sek-1(km4)* animals on control RNAi died within 24 hours of exposure to *P. aeruginosa* (Figure 4A). Importantly, the knockdown of *ufd-1*

resulted in a drastic improvement in the survival of *sek-1(km4)* animals (Figure 4A). To test whether the improved survival of *sek-1(km4)* animals upon the knockdown of *ufd-1* was because of inhibition of the UFD-1-NPL-4 complex, we studied the survival of *sek-1(km4)* animals upon *npl-4* RNAi. The knockdown of *npl-4* also resulted in drastically enhanced survival of *sek-1(km4)* animals (Figure 4A).

Knockdown of both *ufd-1* and *npl-4* in *sek-1(km4)* animals resulted in reduced gut colonization by *P. aeruginosa* compared to control RNAi (Figure 4B and 4C). Because *sek-1(km4)* animals do not have a reduced lifespan on *E. coli* diet (Kim et al., 2002), we studied how inhibition of the UFD-1-NPL-4 complex affected the lifespan of *sek-1(km4)* animals. We reasoned that if the inhibition of the UFD-1-NPL-4 complex truly led to an inflammation-like response, it should result in a reduced lifespan of *sek-1(km4)* animals on *E. coli* despite improving their survival on *P. aeruginosa*. Indeed, the knockdown of *ufd-1* and *npl-4* drastically reduced the lifespan of *sek-1(km4)* animals on *E. coli* HT115 (Figure 4D). These results suggested that inhibition of the UFD-1-NPL-4 complex led to an inflammation-like response, which improves survival of severely immunocompromised animals under infection conditions but reduces survival of such animals under non-infection conditions.

To further establish that inhibition of the UFD-1-NPL-4 complex resulted in the improved survival of severely immunocompromised animals on *P. aeruginosa*, we created a *dbl-1(nk3);pmk-1(km25)* double mutant. The TGF-β/DBL-1 and p38 MAPK/PMK-1 control immunity via parallel pathways (Singh and Aballay, 2020), and the *dbl-1(nk3);pmk-1(km25)* animals show reduced survival on *P. aeruginosa* compared to individual mutants (Figure 4E). The knockdown of *ufd-1* resulted in improved survival (Figure 4E) and reduced colonization (Figure 4F and 4G) of *dbl-1(nk3);pmk-1(km25)* animals on *P. aeruginosa*. Taken together, these data showed that inhibition of the UFD-1-NPL-4 complex improved the survival of severely immunocompromised animals on *P. aeruginosa*.

Knockdown of *ufd-1* results in the upregulation of protease and intracellular pathogen response genes

To understand the molecular basis of the phenotypes observed upon knockdown of *ufd-1*, we used RNA sequencing to focus on transcriptional changes induced by *ufd-1* RNAi. Of the 439 differentially regulated genes, 319 were upregulated, while 120 were down-regulated (Figure 5A and Table S1). Gene ontology (GO) analysis for biological processes for upregulated genes showed enrichment for innate immune response (Figure 5B). As *ufd-1* is required for ERAD, different ER-UPR pathway genes were also enriched in the upregulated genes. In

addition, enrichment for proteolysis genes was also observed. GO analysis for cellular components and molecular function for upregulated genes showed enrichment for lysosomes and peptidase activities, respectively (Figure 5C and 5D). These results indicated that the knockdown of *ufd-1* might result in increased proteolysis activities via lysosomes. GO analysis for biological processes for downregulated genes also showed enrichment for innate immune response (Figure S4A). This indicated that *ufd-1* might be required for the expression of some innate immune response genes. GO analysis for cellular components and molecular function for downregulated genes primarily identified functions related to nucleosomes (Figure S4B and S4C). Indeed, UFD-1 is known to localize to the nucleus and is required for chromatin stability (Mouysset et al., 2008).

Next, we compared the upregulated genes with previously published gene expression data using WormExp (Yang et al., 2016b). Interestingly, we observed that the *ufd-1* RNAi upregulated genes had a very high overlap with genes upregulated by intracellular pathogens *Nematocida parisii* (Bakowski et al., 2014) (Figure 5E) and Orsay virus (Sarkies et al., 2013) (Figure 5F). Infection with the intracellular pathogens *N. parisii* and Orsay virus results in the activation of an intracellular pathogen response (IPR), which includes several *p*rotein containing *ALS*2CR12 signature (*pals*) genes as well as genes involved in proteolysis (Bakowski et al., 2014; Sarkies et al., 2013). Indeed, *ufd-1* RNAi resulted in the upregulation of several *pals* and proteolysis genes (Table S1). These results indicated that the knockdown of *ufd-1* might mimic an intracellular pathogen infection and result in the activation of the IPR.

GATA transcription factor ELT-2 mediates the *ufd-1* knockdown phenotypes

To identify the genes downstream of *ufd-1* knockdown that were responsible for reduced colonization, we knocked down individual genes that were upregulated upon *ufd-1* RNAi and studied colonization of the gut with *P. aeruginosa*. We hypothesized that the reduced colonization might be because of increased expression of proteolysis genes. Therefore, we knocked down the proteolysis genes that were upregulated by *ufd-1* RNAi. Knockdown of none of the protease genes led to increased colonization in *ufd-1* knockdown animals (Figure S5A). Because *ufd-1* knockdown also resulted in the upregulation of several *pals* genes, which are part of the IPR, we next targeted the *pals* genes upregulated by *ufd-1* RNAi. Knockdown of none of the *pals* genes led to increased colonization in *ufd-1* knockdown animals (Figure S5B). These results indicated that either the proteases and IPR genes are not

involved in the regulation of colonization in *ufd-1* knockdown animals, or these genes function redundantly, and multiple genes are required for the phenotype.

To identify the transcription factors that regulate the diminished colonization and reduced survival phenotype of *ufd-1* knockdown, we carried out transcription factor enrichment analysis for upregulated genes using WormExp. The *ufd-1* RNAi upregulated genes substantially overlapped with the genes regulated by the GATA transcription factor ELT-2 (Dineen et al., 2018; Mann et al., 2016) (Figure 6A and 6B). Indeed, ELT-2 is known to regulate protease and *pals* genes (Mann et al., 2016). To test whether ELT-2 might be required for the *ufd-1* knockdown phenotypes, we studied *P. aeruginosa* colonization in N2 animals upon the knockdown of *ufd-1* and *elt-2*. Knockdown of *elt-2* resulted in a significant increase in *P. aeruginosa* colonization in *ufd-1* knockdown animals (Figure 6C and 6D). Similar to N2 worms, the knockdown of *elt-2* resulted in a significant increase in *P. aeruginosa* colonization in *ufd-1* knockdown *sek-1(km4)* animals (Figure 6E and 6F). Because *ufd-1* knockdown in *sek-1(km4)* worms improves their survival on *P. aeruginosa* (Figure 4A), we also studied whether *elt-2* was responsible for the increased survival of *sek-1(km4)* worms upon *ufd-1* knockdown. Indeed, the knockdown of *elt-2* abolished the beneficial effects of *ufd-1* knockdown on the survival of *sek-1(km4)* worms on *P. aeruginosa* (Figure 6G). Taken together, these results indicated that the inflammation-like response triggered by the inhibition of the UFD-1-NPL-4 complex is mediated by ELT-2.

Discussion

In this study, we show that inhibition of the UFD-1-NPL-4 complex leads to an inflammation-like response in *C. elegans*. Inhibition of the UFD-1-NPL-4 complex leads to reduced gut colonization with *P. aeruginosa* in wild-type animals as well as mutants of different ER-UPR and immunity pathways. Despite the reduction in pathogen colonization, the wild-type animals exhibit reduced survival, indicating an inflammatory response. However, immunocompromised mutants, which have drastically reduced survival on pathogenic bacteria, exhibit reduced colonization and improved survival on inhibition of the UFD-1-NPL-4 complex. This indicates that the inflammatory response activated by the inhibition of the UFD-1-NPL-4 complex compensates for the dampened immune response of the immunocompromised mutants. Despite beneficial effects on the survival on pathogenic bacteria, inhibition of the UFD-1-NPL-4 complex leads to adverse effects on the lifespan of immunocompromised mutants. This is because the immunocompromised mutants have a

normal lifespan on nonpathogenic bacteria, and the inflammatory response becomes detrimental on such bacterial diets.

We find that the knockdown of *ufd-1* led to the upregulation of several genes that are part of the IPR activated by intracellular pathogens *N. parisii* and Orsay virus (Bakowski et al., 2014; Sarkies et al., 2013). The ubiquitination components have been shown to be required for targeting the intracellular pathogen *N. parisii* (Bakowski et al., 2014). As a counterattack, the pathogen probably targets the ubiquitin-proteasome system of the host (Bakowski et al., 2014). Therefore, the intracellular pathogens *N. parisii* and Orsay virus might activate the IPR by inhibiting the ubiquitin-proteasome system (Bakowski et al., 2014; Reddy et al., 2019). We show that inhibition of the UFD-1-NPL-4 complex activates the IPR. The activation of the IPR by the inhibition of the UFD-1-NPL-4 complex could be a consequence of the direct inhibition of this complex itself or an indirect perturbation of the proteasomal degradation of proteins. In future studies, it will be intriguing to decipher whether intracellular pathogens target the UFD-1-NPL-4 complex.

We demonstrate that the GATA transcription factor ELT-2 mediated the inflammatory response downstream of the inhibition of the UFD-1-NPL-4 complex. ELT-2 is known to be required for defense as well as recovery responses against a variety of pathogens (Head and Aballay, 2014; Shapira et al., 2006; Yang et al., 2016a). Previous studies have reported interactions of ELT-2 with the proteasome system. The non-proteolytic activity of the 19S proteasome subunit RPT-6 was shown to regulate the ELT-2-mediated immune response (Olaitan and Aballay, 2018). Another study showed that the bacterial pathogen *Burkholderia pseudomallei* leads to the downregulation of ELT-2 target genes (Lee et al., 2013). It was demonstrated that the downregulation of ELT-2 targets was associated with the degradation of ELT-2 protein by the host ubiquitin-proteasome system. Therefore, multiple mechanisms could regulate the activity of ELT-2 via the ubiquitin-proteasome system. In future studies, it will be interesting to study how inhibition of the UFD-1-NPL-4 complex modulates the activities of the GATA transcription factor ELT-2.

Materials and Methods

Bacterial strains

The following bacterial strains were used in the current study: *Escherichia coli* OP50, *E. coli* HT115(DE3), *Pseudomonas aeruginosa* PA14, and *P. aeruginosa* PA14 expressing green fluorescent protein (*P. aeruginosa* PA14-GFP). The cultures of *E. coli* OP50, *E. coli* HT115(DE3), and *P. aeruginosa* PA14 were grown in Luria-Bertani (LB) broth at 37°C. The

P. aeruginosa PA14-GFP cultures were grown in LB broth with 50 µg/mL kanamycin at 37°C.

C. elegans strains and growth conditions

C. elegans hermaphrodites were maintained at 20°C on nematode growth medium (NGM) plates seeded with *E. coli* OP50 as the food source unless otherwise indicated. Bristol N2 was used as the wild-type control unless otherwise indicated. The following strains were used in the study: KU4 *sek-1(km4)*, KU25 *pmk-1(km25)*, NU3 *dbl-1(nk3)*, JIN1375 *hlh-30(tm1978)*, *xbp-1(tm2482)*, RB545 *pek-1(ok275)*, RB772 *atf-6(ok551)*, and RB1085 *tir-1(qd4)*. Some of the strains were obtained from the Caenorhabditis Genetics Center (University of Minnesota, Minneapolis, MN). The *dbl-1(nk3);pmk-1(km25)* strain was obtained by a standard genetic cross.

Construction of the _npl-4_ RNAi clone

The 1581-base-pair full-length cDNA of *npl-4.1* was amplified using the forward primer 5'-GCTCCCGGGATGGTACTTGAAGTCCCTCA -3' and the reverse primer 5'-AGGTCTAGAATCGGCAGCTGGCAATCCAC -3'. Because the nucleotide sequence of the *npl-4.1* gene is 99% identical to that of the *npl-4.2* gene, the cloned cDNA will target both of these genes. Therefore, the clone is referred to as *npl-4*. The fragment was cloned into the SmaI and XbaI sites of pL4440 (Open Biosystems) and transformed into *E. coli* HT115(DE3) cells.

RNA interference (RNAi)

RNAi was used to generate loss-of-function phenotypes by feeding worms with *E. coli* strain HT115(DE3) expressing double-stranded RNA homologous to a target *C. elegans* gene. RNAi was carried out as described previously (Das et al., 2023). Briefly, *E. coli* HT115(DE3) with the appropriate vectors were grown in LB broth containing ampicillin (100 µg/mL) at 37°C overnight on a shaker, concentrated ten times, and plated onto RNAi NGM plates containing 100 µg/mL ampicillin and 3 mM isopropyl β-D-thiogalactoside (IPTG). The plated bacteria were allowed to grow overnight at 37°C. For synchronization of worms, gravid adults were transferred to RNAi-expressing bacterial lawns and allowed to lay eggs for 2 hours. The gravid adults were removed, and the eggs were developed at 20°C for 96 hours. For protease and IPR genes co-RNAi with *ufd-1*, *E. coli* HT115(DE3) with the appropriate vectors were grown separately at 37°C overnight until growth saturation. Then,

the RNAi cultures were mixed in a ratio of 1:1, concentrated ten times, and plated onto RNAi plates, followed by overnight growth at 37°C. We used all the protease and *pals* genes that were upregulated upon *ufd-1* RNAi and were present in the Ahringer RNAi library. For experiments involving *elt-2* RNAi, the worms were grown on the control empty vector (EV) and *ufd-1* RNAi for 48 hours at 20°C to obtain the L4 stage worms. Afterward, the worms grown on EV were transferred to EV+*elt-2* RNAi plates, and those grown on *ufd-1* RNAi were transferred to EV+*ufd-1* and *ufd-1*+*elt-2* RNAi plates. This was followed by the incubation of the worms at 20°C for another 48 hours before transferring to *P. aeruginosa* plates.

C. elegans killing assay on _P. aeruginosa_ PA14

The full-lawn killing assays of *C. elegans* on *P. aeruginosa* PA14 were carried out as described earlier (Singh and Aballay, 2019a). Briefly, *P. aeruginosa* PA14 cultures were grown by inoculating individual bacterial colonies into 2 mL of LB broth and growing them for 8–10 hours on a shaker at 37°C. Then, 20 µL of the culture was spread on the complete surface of 3.5-cm-diameter standard slow-killing (SK) plates (modified NGM agar plates (0.35% instead of 0.25% peptone)). The plates were incubated at 37°C for 12-16 hours and then cooled to room temperature for at least 30 min before seeding with synchronized gravid adult hermaphrodite worms. The killing assays were performed at 25°C, and live animals were transferred to fresh plates after every 24 hours. Animals were scored at the indicated times and considered dead when they failed to respond to touch. At least three independent experiments were performed for each condition.

P. aeruginosa-GFP colonization assay

The *P. aeruginosa* PA14-GFP colonization assays were carried out as described earlier (Das et al., 2023; Singh and Aballay, 2019b). Briefly, bacterial cultures were prepared by inoculating individual bacterial colonies into 2 mL of LB broth containing 50 µg/mL kanamycin and growing them for 8-10 hours on a shaker at 37°C. Then, 20 µL of the culture was spread on the complete surface of 3.5-cm-diameter SK plates containing 50 µg/mL kanamycin. The plates were incubated at 37°C for 12-16 hours and then cooled to room temperature for at least 30 min before seeding with gravid adult hermaphrodite worms. The assays were performed at 25°C. At indicated times, the worms were picked under a non-fluorescence stereomicroscope and visualized within 5 minutes under a fluorescence microscope.

Quantification of intestinal bacterial loads

The quantification of intestinal *P. aeruginosa* PA14-GFP load was carried by measuring colony-forming units (CFU) as described earlier (Das et al., 2023). Briefly, *P. aeruginosa* PA14-GFP lawns were prepared as described above. At the indicated times for each experiment, the animals were transferred from *P. aeruginosa*-GFP plates to the center of fresh *E. coli* OP50 plates thrice for 10 minutes each to eliminate bacteria stuck to their body. Afterward, ten animals/condition were transferred into 50 μL of PBS containing 0.01% triton X-100 and ground using glass beads. Serial dilutions of the lysates (10^1, 10^2, 10^3, 10^4) were seeded onto LB plates containing 50 μg/mL of kanamycin to select for *P. aeruginosa*-GFP cells and grown overnight at 37°C. Single colonies were counted the next day and represented as the number of bacterial cells or CFU per animal. Six independent experiments were performed for each condition.

Pharyngeal Pumping Assay

For the pharyngeal pumping assay without *P. aeruginosa* PA14 exposure, wild-type N2 animals were grown on appropriate RNAi clones till 1-day-old adults before the measurements. For the pharyngeal pumping assay with *P. aeruginosa* PA14 exposure, wild-type N2 animals were grown on appropriate RNAi clones till 1-day-old adults, followed by exposure to *P. aeruginosa* PA14 for 12 hours at 25°C before measurements. The number of contractions of the terminal bulb of the pharynx was counted for 30 seconds per worm. The pumping rates for at least 30 worms were recorded for each condition.

***C. elegans* lifespan assays**

Lifespan assays were performed as described earlier (Das et al., 2023). Briefly, the assays were performed on RNAi plates containing *E. coli* HT115(DE3) with appropriate vectors in the presence of 50 μg/mL of 5-fluorodeoxyuridine (FUdR). Animals were synchronized on RNAi plates without FUdR and incubated at 20°C. At the late L4 larval stage, the animals were transferred onto the corresponding RNAi plates containing 50 μg/mL of FUdR and incubated at 20°C. Animals were scored every day as live, dead, or gone. Animals that failed to display touch-provoked movement were scored as dead. Animals that crawled off the plates were censored. Experimental groups contained more than 60 animals per condition per replicate. Young adult animals were considered as day 0 for the lifespan analysis. Three independent experiments were performed.

RNA isolation

RNA isolation was carried out as described earlier (Singh and Aballay, 2017). Briefly, animals were synchronized by egg laying. Approximately 35 N2 gravid adult animals were transferred to 10-cm RNAi plates seeded with *E. coli* HT115 expressing the appropriate vectors and allowed to lay eggs for 4 hours. The gravid adults were then removed, and the eggs were allowed to develop at 20°C for 96 hours. The animals were then collected, washed with M9 buffer, and frozen in TRIzol reagent (Life Technologies, Carlsbad, CA). Total RNA was extracted using the RNeasy Plus Universal Kit (Qiagen, Netherlands). Residual genomic DNA was removed using TURBO DNase (Life Technologies, Carlsbad, CA).

RNA sequencing and data analysis

Total RNA samples for N2 animals grown on control empty vector and *ufd-1* RNAi were isolated from three biological replicates as described above. Library preparation and sequencing were performed at the Novogene Corporation Inc, USA. The cDNA libraries were sequenced on HiseqX sequencing platform using 150 bp paired-end nucleotide reads.

The RNA sequence data were analyzed using the web platform Galaxy (https://usegalaxy.org/). The paired reads were first trimmed using the Trimmomatic tool. The trimmed reads obtained for each sample were mapped to the *C. elegans* genome (WS220) using the aligner STAR. The number of reads mapped to each gene was counted using the *htseq-count* tool. Differential gene expression analysis was then performed using DESeq2. Genes exhibiting at least two-fold change and *P*-value <0.01 were considered differentially expressed. Gene ontology analysis was performed using the DAVID Bioinformatics Database (https://david.ncifcrf.gov/tools.jsp). The overlap of the upregulated genes with previously published datasets was carried out with WormExp v 2.0 (https://wormexp.zoologie.uni-kiel.de/wormexp/) (Yang et al., 2016b). The Venn diagrams were obtained using the web tool BioVenn (https://www.biovenn.nl/) (Hulsen et al., 2008).

Fluorescence imaging

Fluorescence imaging was carried out as described previously (Gokul and Singh, 2022; Ravi et al., 2023). Briefly, the animals were anesthetized using an M9 salt solution containing 50 mM sodium azide and mounted onto 2% agarose pads. The animals were then visualized using a Nikon SMZ-1000 fluorescence stereomicroscope. The fluorescence intensity was quantified using Image J software.

Quantification and statistical analysis

The statistical analysis was performed with Prism 8 (GraphPad). All error bars represent mean±standard deviation (SD). The two-sample *t*-test was used when needed, and the data were judged to be statistically significant when $p < 0.05$. In the figures, asterisks (*) denote statistical significance as follows: *, $p<0.05$, **, $p<0.01$, ***, $p<0.001$, as compared with the appropriate controls. The Kaplan-Meier method was used to calculate the survival fractions, and statistical significance between survival curves was determined using the log-rank test. All experiments were performed in triplicate.

Acknowledgments

Some strains used in this study were provided by the Caenorhabditis Genetics Center (CGC), which is funded by the NIH Office of Research Infrastructure Programs (P40 OD010440).

Funding: This work was supported by the following grants: Ramalingaswami Re-entry Fellowship (Ref. No. BT/RLF/Re-entry/50/2020) awarded by the Department of Biotechnology, India, STARS grant (File No. MoE-STARS/STARS-2/2023-0116) awarded by the Ministry of Education, India, Startup Research Grant, SERB (Ref. No. SRG/2020/000022) awarded by DST, India, and IISER Mohali intramural funds. R.R. was supported by a junior research fellowship from the Council of Scientific & Industrial Research (CSIR), India.

Author contributions

Rajneesh Rao: Conceptualization, Data curation, Formal analysis, Investigation, Methodology, Visualization

Alejandro Aballay: Conceptualization, Visualization, Supervision

Jogender Singh: Conceptualization, Data curation, Formal analysis, Funding acquisition, Investigation, Methodology, Project administration, Visualization, Supervision, Writing—original draft, Writing— review and editing

Competing interest: The authors declare that they have no competing interest.

Data Availability: The RNA sequencing data for N2 worms grown on empty vector control and *ufd-1* RNAi have been submitted to the public repository, the Sequence Read Archive,

with BioProject ID PRJNA1033335. All data generated or analyzed during this study are included in the manuscript and supporting files.

References

Amrit FRG, Naim N, Ratnappan R, Loose J, Mason C, Steenberge L, McClendon BT, Wang G, Driscoll M, Yanowitz JL, Ghazi A. 2019. The longevity-promoting factor, TCER-1, widely represses stress resistance and innate immunity. *Nat Commun* **10**:3042. doi:10.1038/s41467-019-10759-z

Bakowski MA, Desjardins CA, Smelkinson MG, Dunbar TA, Lopez-Moyado IF, Rifkin SA, Cuomo CA, Troemel ER. 2014. Ubiquitin-Mediated Response to Microsporidia and Virus Infection in C. elegans. *PLoS Pathog* **10**. doi:10.1371/journal.ppat.1004200

Bodnar NO, Rapoport TA. 2017. Molecular Mechanism of Substrate Processing by the Cdc48 ATPase Complex. *Cell* **169**:722–735. doi:10.1016/j.cell.2017.04.020

Bomberger JM, Ye S, Maceachran DP, Koeppen K, Barnaby RL, Toole GAO, Stanton BA. 2011. A Pseudomonas aeruginosa Toxin that Hijacks the Host Ubiquitin Proteolytic System. *PLoS Pathog* **7**:e1001325. doi:10.1371/journal.ppat.1001325

Boom J Van Den, Meyer H. 2018. VCP/p97-Mediated Unfolding as a Principle in Protein Homeostasis and Signaling. *Mol Cell* **69**:182–194. doi:10.1016/j.molcel.2017.10.028

Chai Q, Wang X, Qiang L, Zhang Y, Ge P, Lu Z, Zhong Y, Li B, Wang J, Zhang L, Zhou D, Li W, Dong W, Pang Y, Gao GF, Liu CH. 2019. A Mycobacterium tuberculosis surface protein recruits ubiquitin to trigger host xenophagy. *Nat Commun* **10**:1973. doi:10.1038/s41467-019-09955-8

Clague MJ, Urbe S. 2010. Ubiquitin: Same Molecule, Different Degradation Pathways. *Cell* **143**:682–685. doi:10.1016/j.cell.2010.11.012

Das P, Aballay A, Singh J. 2023. Calcineurin inhibition enhances Caenorhabditis elegans lifespan by defecation defects-mediated calorie restriction and nuclear hormone signaling. *Elife* **12**:RP89572.

Dikic I. 2017. Proteasomal and Autophagic Degradation Systems. *Annu Rev Biochem* **86**:193–224.

Dineen A, Osborne E, Goszczynski B, Rothman JH, Mcghee JD. 2018. Quantitating

transcription factor redundancy: The relative roles of the ELT-2 and ELT-7 GATA factors in the C. elegans endoderm. *Dev Biol* **435**:150–161. doi:10.1016/j.ydbio.2017.12.023

Ding W-X, Yin X-M. 2008. Sorting, recognition and activation of the misfolded protein degradation pathways through macroautophagy and the proteasome. *Autophagy* **4**:141–150. doi:10.4161/auto.5190

Engel A, Barton GM. 2010. Unfolding new roles for XBP1 in immunity. *Nat Immunol* **11**:365–367. doi:10.1038/ni0510-365

Garcia-Sanchez JA, Ewbank JJ, Visvikis O. 2021. Ubiquitin-related processes and innate immunity in C. elegans. *Cell Mol Life Sci* **78**:4305–4333. doi:10.1007/s00018-021-03787-w

Gokul G, Singh J. 2022. Dithiothreitol causes toxicity in C. elegans by modulating the methionine-homocysteine cycle. *Elife* **11**:e76021. doi:10.7554/eLife.76021

Haldar AK, Foltz C, Finethy R, Piro AS, Feeley EM, Pilla-moffett DM, Komatsuc M, Frickelb E-M, Coers J. 2015. Ubiquitin systems mark pathogen-containing vacuoles as targets for host defense by guanylate binding proteins. *Proc Natl Acad Sci U S A* **112**:E5628–E5637. doi:10.1073/pnas.1515966112

Head B, Aballay A. 2014. Recovery from an Acute Infection in C. elegans Requires the GATA Transcription Factor ELT-2. *PLoS Genet* **10**. doi:10.1371/journal.pgen.1004609

Herhaus L, Dikic I. 2018. Regulation of Salmonella -host cell interactions via the ubiquitin system. *Int J Med Microbiol* **308**:176–184. doi:10.1016/j.ijmm.2017.11.003

Hetz C, Chevet E, Oakes SA. 2015. Proteostasis control by the unfolded protein response. *Nat Cell Biol* **17**:829–838. doi:10.1038/ncb3184

Hulsen T, de Vlieg J, Alkema W. 2008. BioVenn - A web application for the comparison and visualization of biological lists using area-proportional Venn diagrams. *BMC Genomics* **9**:488. doi:10.1186/1471-2164-9-488

Husnjak K, Dikic I. 2012. Ubiquitin-Binding Proteins: Decoders of Ubiquitin- Mediated Cellular Functions. *Annu Rev Biochem* **81**:291–322. doi:10.1146/annurev-biochem-051810-094654

Kim DH, Feinbaum R, Alloing G, Emerson FE, Garsin DA, Inoue H, Tanaka-Hino M, Hisamoto N, Matsumoto K, Tan M-W, Ausubel FM. 2002. A Conserved p38 MAP Kinase Pathway in Caenorhabditis elegans Innate Immunity. *Science (80-)* **297**:623–626. doi:10.1126/science.1073759

Lee S, Wong R, Chin C, Lim T, Eng S, Kong C, Ijap NA, Lau M-S, Lim M-P, Gan Y-H, He F-L, Tan M-W, Nathan S. 2013. Burkholderia pseudomallei suppresses Caenorhabditis elegans immunity by specific degradation of a GATA transcription factor. *Proc Natl Acad Sci* **110**:15067–15072. doi:10.1073/pnas.1311725110

Li J, Chai Q-Y, Liu CH. 2016. The ubiquitin system: a critical regulator of innate immunity and pathogen–host interactions. *Cell Mol Immunol* **13**:560–576. doi:10.1038/cmi.2016.40

Liberati NT, Fitzgerald KA, Kim DH, Feinbaum R, Golenbock DT, Ausubel FM. 2004. Requirement for a conserved Toll/interleukin-1 resistance domain protein in the Caenorhabditis elegans immune response. *Proc Natl Acad Sci* **101**:6593–6598. doi:10.1073/pnas.0308625101

Mallo G V, Le C, Couillault C, Pujol N, Granjeaud S, Kohara Y, Ewbank JJ. 2002. Inducible Antibacterial Defense System in C. elegans. *Curr Biol* **12**:1209–1214.

Mann FG, Nostrand EL Van, Friedland AE, Liu X, Kim SK. 2016. Deactivation of the GATA Transcription Factor ELT-2 Is a Major Driver of Normal Aging in C. elegans. *PLoS Genet* **12**:e1005956. doi:10.1371/journal.pgen.1005956

Meng J, Fu L, Liu K, Tian C, Wu Z, Jung Y, Ferreira RB, Carroll KS, Blackwell TK, Yang J. 2021. Global profiling of distinct cysteine redox forms reveals wide-ranging redox regulation in C. elegans. *Nat Commun* **12**:1415. doi:10.1038/s41467-021-21686-3

Meyer H, Bug M, Bremer S. 2012. Emerging functions of the VCP / p97 AAA-ATPase in the ubiquitin system. *Nat Cell Biol* **14**:117–123. doi:10.1038/ncb2407

Meyer HH, Shorter JG, Seemann J, Pappin D, Warren G. 2000. A complex of mammalian Ufd1 and Npl4 links the AAA-ATPase, p97, to ubiquitin and nuclear transport pathways. *EMBO J* **19**:2181–2192. doi:10.1093/emboj/19.10.2181

Mouysset J, Deichsel A, Moser S, Hoege C, Hyman AA, Gartner A, Hoppe T. 2008. Cell cycle progression requires the CDC-48UFD-1/NPL-4 complex for efficient DNA

replication. *Proc Natl Acad Sci U S A* **105**:12879–12884. doi:10.1073/pnas.0805944105

Mouysset J, Kähler C, Hoppe T. 2006. A conserved role of Caenorhabditis elegans CDC-48 in ER-associated protein degradation. *J Struct Biol* **156**:41–49. doi:10.1016/j.jsb.2006.02.015

Mukhopadhyay D, Riezman H. 2007. Proteasome-Independent Functions of Ubiquitin in Endocytosis and Signaling. *Science (80-)* **315**:201–205.

Olaitan AO, Aballay A. 2018. Non-proteolytic activity of 19S proteasome subunit RPT-6 regulates GATA transcription during response to infection. *PLoS Genet* **14**:e1007693.

Otarigho B, Aballay A. 2021. Immunity-longevity tradeoff neurally controlled by GABAergic transcription factor PITX1/UNC-30. *Cell Rep* **35**:109187. doi:10.1016/j.celrep.2021.109187

Otten EG, Werner E, Crespillo-casado A, Boyle KB, Dharamdasani V, Pathe C, Santhanam B, Randow F. 2021. Ubiquitylation of lipopolysaccharide by RNF213 during bacterial infection. *Nature* **594**:111–116. doi:10.1038/s41586-021-03566-4

Peterson ND, Icso JD, Salisbury JE, Rodríguez T, Thompson PR, Pukkila-Worley R. 2022. Pathogen infection and cholesterol deficiency activate the C. elegans p38 immune pathway through a TIR-1/SARM1 phase transition. *Elife* **11**:e74206.

Ravi, Kumar A, Bhattacharyya S, Singh J. 2023. Thiol reductive stress activates the hypoxia response pathway. *EMBO J* **42**:e114093. doi:10.15252/embj.2023114093

Reddy KC, Dror T, Underwood RS, Osman GA, Elder CR, Desjardins CA, Cuomo CA, Barkoulas M, Troemel ER. 2019. Antagonistic paralogs control a switch between growth and pathogen resistance in C. elegans. *PLoS Pathog* **15**:e1007528. doi:10.1371/journal.ppat.1007528

Ren Z, Ambros VR. 2015. Caenorhabditis elegans microRNAs of the let-7 family act in innate immune response circuits and confer robust developmental timing against pathogen stress. *Proc Natl Acad Sci U S A* **112**:E2366–E2375. doi:10.1073/pnas.1422858112

Ribet D, Cossart P. 2018. Ubiquitin, SUMO, and NEDD8: Key Targets of Bacterial Pathogens. *Trends Cell Biol* **28**:926–940. doi:10.1016/j.tcb.2018.07.005

Richardson CE, Kooistra T, Kim DH. 2010. An essential role for XBP-1 in host protection against immune activation in C. elegans. *Nature* **463**:1092–1095. doi:10.1038/nature08762

Sarkies P, Ashe A, Pen J Le, Mckie MA, Miska EA. 2013. Competition between virus-derived and endogenous small RNAs regulates gene expression in Caenorhabditis elegans. *Genome Res* **23**:1258–1270. doi:10.1101/gr.153296.112

Sasagawa Y, Yamanaka K, Ogura T. 2007. ER E3 ubiquitin ligase HRD-1 and its specific partner chaperone BiP play important roles in ERAD and developmental growth in Caenorhabditis elegans. *Genes to Cells* **12**:1063–1073. doi:10.1111/j.1365-2443.2007.01108.x

Shapira M, Hamlin BJ, Rong J, Chen K, Ronen M, Tan M-W. 2006. A conserved role for a GATA transcription factor in regulating epithelial innate immune responses. *Proc Natl Acad Sci U S A* **103**:14086–91. doi:10.1073/pnas.0603424103

Singh J. 2023. ERASing endoplasmic reticulum stress: the faster, the better. *Trends Cell Biol* **33**:179–181. doi:10.1016/j.tcb.2022.12.003

Singh J, Aballay A. 2020. Neural control of behavioral and molecular defenses in C. elegans. *Curr Opin Neurobiol* **62**:34–40. doi:10.1016/j.conb.2019.10.012

Singh J, Aballay A. 2019a. Intestinal infection regulates behavior and learning via neuroendocrine signaling. *Elife* **8**:e50033. doi:10.7554/eLife.50033

Singh J, Aballay A. 2019b. Microbial colonization activates an immune fight-and-flight response via neuroendocrine signaling. *Dev Cell* **49**:89–99. doi:10.1016/j.devcel.2019.02.001

Singh J, Aballay A. 2017. Endoplasmic reticulum stress caused by lipoprotein accumulation suppresses immunity against bacterial pathogens and contributes to immunosenescence. *MBio* **8**:e00778-17. doi:10.1128/mBio.00778-17

Sun J, Liu Y, Aballay A. 2012. Organismal regulation of XBP-1-mediated unfolded protein response during development and immune activation. *EMBO Rep* **13**:855–860. doi:10.1038/embor.2012.100

Tan MW, Mahajan-Miklos S, Ausubel FM. 1999. Killing of Caenorhabditis elegans by Pseudomonas aeruginosa used to model mammalian bacterial pathogenesis. *Proc Natl*

Acad Sci U S A **96**:715–20. doi:10.1073/pnas.96.2.715

Tripathi-Giesgen I, Behrends C, Alpi AF. 2021. The ubiquitin ligation machinery in the defense against bacterial pathogens. *EMBO Rep* **22**:e52864. doi:10.15252/embr.202152864

Vembar SS, Brodsky JL. 2008. One step at a time: endoplasmic reticulum-associated degradation. *Nat Rev Mol Cell Biol* **9**:944–957. doi:10.1038/nrm2546

Vilchez D, Saez I, Dillin A. 2014. The role of protein clearance mechanisms in organismal ageing and age-related diseases. *Nat Commun* **5**:5659. doi:10.1038/ncomms6659

Visvikis O, Ihuegbu N, Labed SA, Luhachack LG, Alves AMF, Wollenberg AC, Stuart LM, Stormo GD, Irazoqui JE. 2014. Innate host defense requires TFEB-mediated transcription of cytoprotective and antimicrobial genes. *Immunity* **40**:896–909. doi:10.1016/j.immuni.2014.05.002

Wolf DH, Stolz A. 2012. The Cdc48 machine in endoplasmic reticulum associated protein degradation . *Biochim Biophys Acta* **1823**:117–124. doi:10.1016/j.bbamcr.2011.09.002

Wu X, Rapoport TA. 2018. Mechanistic insights into ER-associated protein degradation. *Curr Opin Cell Biol* **53**:22–28. doi:10.1016/j.ceb.2018.04.004

Yang W, Dierking K, Rosenstiel PC, Schulenburg H. 2016a. GATA transcription factor as a likely key regulator of the Caenorhabditis elegans innate immune response against gut pathogens. *Zoology* **119**:244–253. doi:10.1016/j.zool.2016.05.013

Yang W, Dierking K, Schulenburg H. 2016b. WormExp: A web-based application for a Caenorhabditis elegans-specific gene expression enrichment analysis. *Bioinformatics* **32**:943–945. doi:10.1093/bioinformatics/btv667

Ye Y, Meyer HH, Rapoport TA. 2001. The AAA ATPase Cdc48/p97 and its partners transport proteins from the ER into the cytosol. *Nature* **414**:652–656.

Figures

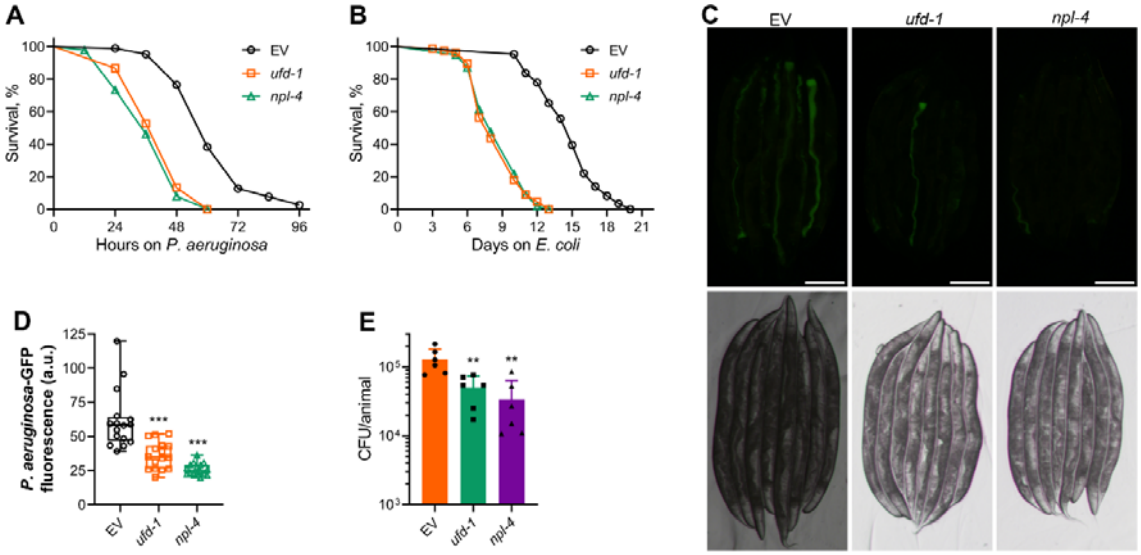

Figure 1. Inhibition of the UFD-1-NPL-4 complex reduces survival of *C. elegans* on *P. aeruginosa*

(A) Representative survival plots of N2 animals on *P. aeruginosa* PA14 at 25°C after treatment with the empty vector (EV) control, *ufd-1*, and *npl-4* RNAi. *P*<0.001 for *ufd-1* and *npl-4* RNAi compared to EV control.

(B) Representative survival plots of N2 animals grown on bacteria for RNAi against *ufd-1* and *npl-4* along with the EV control at 20°C. Day 0 represents young adults. *P*<0.001 for *ufd-1* and *npl-4* RNAi compared to EV control.

(C) Representative fluorescence (top) and the corresponding brightfield (bottom) images of N2 animals incubated on *P. aeruginosa*-GFP for 24 hours at 25°C after growth on the EV control, *ufd-1*, and *npl-4* RNAi bacteria. Scale bar = 200 μm.

(D) Quantification of GFP levels of N2 animals incubated on *P. aeruginosa*-GFP for 24 hours at 25°C after growth on the EV control, *ufd-1*, and *npl-4* RNAi bacteria. ***$P < 0.001$ via the *t*-test ($n = 16$ worms each).

(E) Colony-forming units (CFU) per animal of N2 worms incubated on *P. aeruginosa*-GFP for 24 hours at 25°C after growth on the EV control, *ufd-1*, and *npl-4* RNAi bacteria. **$P < 0.01$ via the *t*-test (n = 6 biological replicates).

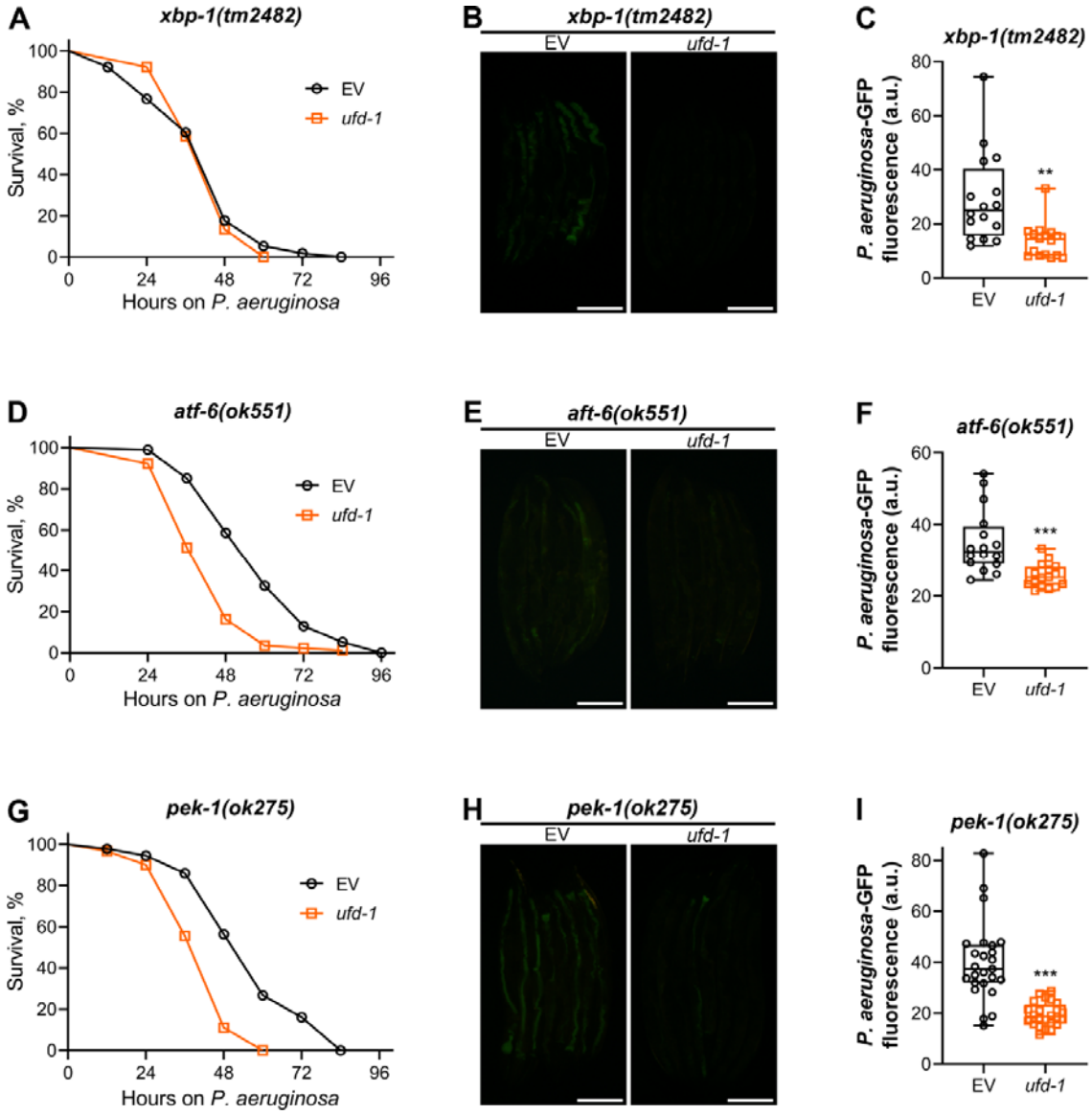

Figure 2. Reduced colonization with *P. aeruginosa* upon *ufd-1* knockdown is independent of the ER-UPR pathways

(A) Representative survival plots of *xbp-1(tm2482)* animals on *P. aeruginosa* PA14 at 25°C after treatment with the empty vector (EV) control and *ufd-1* RNAi. The difference between the EV and *ufd-1* RNAi survival plots is nonsignificant.

(B) Representative fluorescence images of *xbp-1(tm2482)* animals incubated on *P. aeruginosa*-GFP for 24 hours at 25°C after growth on the EV control and *ufd-1* RNAi bacteria. Scale bar = 200 µm.

(C) Quantification of GFP levels of *xbp-1(tm2482)* animals incubated on *P. aeruginosa*-GFP for 24 hours at 25°C after growth on the EV control and *ufd-1* RNAi bacteria. $^{**}P < 0.01$ via the *t*-test ($n = 16$ worms each).

(D) Representative survival plots of *atf-6(ok551)* animals on *P. aeruginosa* PA14 at 25°C after treatment with the EV control and *ufd-1* RNAi. $P<0.001$.

(E) Representative fluorescence images of *atf-6(ok551)* animals incubated on *P. aeruginosa*-GFP for 24 hours at 25°C after growth on the EV control and *ufd-1* RNAi bacteria. Scale bar = 200 μm.

(F) Quantification of GFP levels of *atf-6(ok551)* animals incubated on *P. aeruginosa*-GFP for 24 hours at 25°C after growth on the EV control and *ufd-1* RNAi bacteria. $^{***}P < 0.001$ via the *t*-test ($n = 16$ worms each).

(G) Representative survival plots of *pek-1(ok275)* animals on *P. aeruginosa* PA14 at 25°C after treatment with the EV control and *ufd-1* RNAi. $P<0.001$.

(H) Representative fluorescence images of *pek-1(ok275)* animals incubated on *P. aeruginosa*-GFP for 24 hours at 25°C after growth on the EV control and *ufd-1* RNAi bacteria. Scale bar = 200 μm.

(I) Quantification of GFP levels of *pek-1(ok275)* animals incubated on *P. aeruginosa*-GFP for 24 hours at 25°C after growth on the EV control and *ufd-1* RNAi bacteria. $^{***}P < 0.001$ via the *t*-test ($n = 24$–25 worms each).

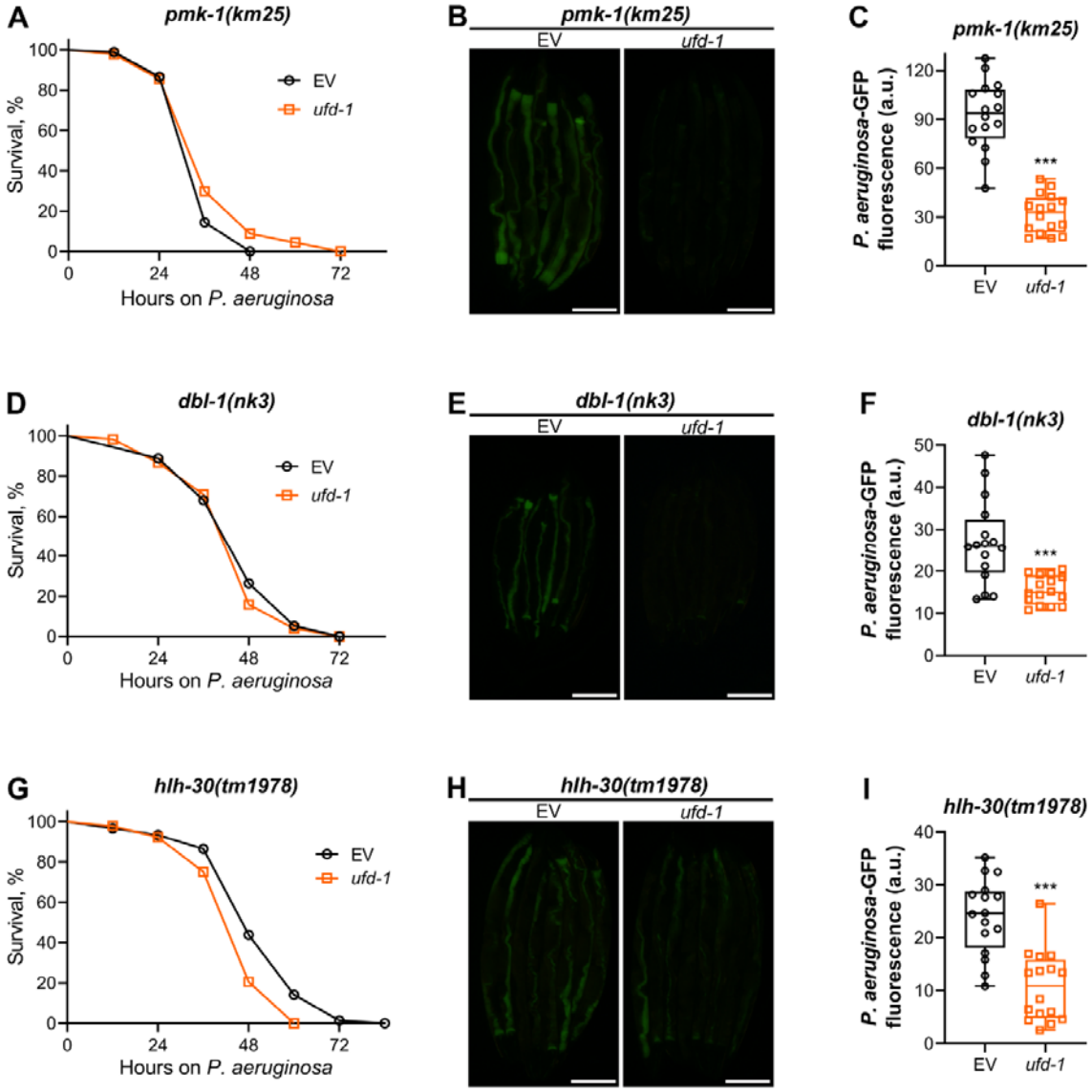

Figure 3. Reduced colonization with *P. aeruginosa* upon *ufd-1* knockdown is independent of the major immunity pathways

(A) Representative survival plots of *pmk-1(km25)* animals on *P. aeruginosa* PA14 at 25°C after treatment with the empty vector (EV) control and *ufd-1* RNAi. The difference between the EV and *ufd-1* RNAi survival plots is nonsignificant.

(B) Representative fluorescence images of *pmk-1(km25)* animals incubated on *P. aeruginosa*-GFP for 24 hours at 25°C after growth on the EV control and *ufd-1* RNAi bacteria. Scale bar = 200 µm.

(C) Quantification of GFP levels of *pmk-1(km25)* animals incubated on *P. aeruginosa*-GFP for 24 hours at 25°C after growth on the EV control and *ufd-1* RNAi bacteria. ***$P < 0.001$ via the *t*-test ($n = 16$ worms each).

(D) Representative survival plots of *dbl-1(nk3)* animals on *P. aeruginosa* PA14 at 25°C after treatment with the EV control and *ufd-1* RNAi. The difference between the EV and *ufd-1* RNAi survival plots is nonsignificant.

(E) Representative fluorescence images of *dbl-1(nk3)* animals incubated on *P. aeruginosa*-GFP for 24 hours at 25°C after growth on the EV control and *ufd-1* RNAi bacteria. Scale bar = 200 μm.

(F) Quantification of GFP levels of *dbl-1(nk3)* animals incubated on *P. aeruginosa*-GFP for 24 hours at 25°C after growth on the EV control and *ufd-1* RNAi bacteria. ***$P < 0.001$ via the *t*-test ($n = 16$ worms each).

(G) Representative survival plots of *hlh-30(tm1978)* animals on *P. aeruginosa* PA14 at 25°C after treatment with the EV control and *ufd-1* RNAi. $P<0.001$.

(H) Representative fluorescence images of *hlh-30(tm1978)* animals incubated on *P. aeruginosa*-GFP for 24 hours at 25°C after growth on the EV control and *ufd-1* RNAi bacteria. Scale bar = 200 μm.

(I) Quantification of GFP levels of *hlh-30(tm1978)* animals incubated on *P. aeruginosa*-GFP for 24 hours at 25°C after growth on the EV control and *ufd-1* RNAi bacteria. ***$P < 0.001$ via the *t*-test ($n = 16$ worms each).

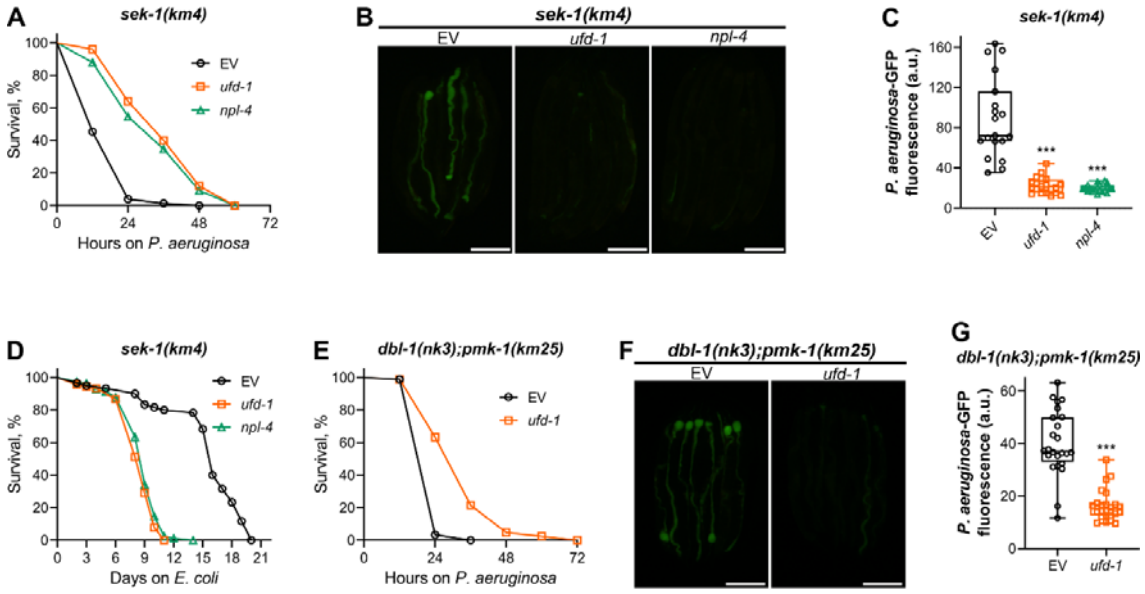

Figure 4. Inhibition of the UFD-1-NPL-4 complex improves survival of severely immunocompromised *C. elegans* on *P. aeruginosa*

(A) Representative survival plots of *sek-1(km4)* animals on *P. aeruginosa* PA14 at 25°C after treatment with the empty vector (EV) control, *ufd-1*, and *npl-4* RNAi. $P<0.001$ for *ufd-1* and *npl-4* RNAi compared to EV control.

(B) Representative fluorescence images of *sek-1(km4)* animals incubated on *P. aeruginosa*-GFP for 12 hours at 25°C after growth on the EV control, *ufd-1*, and *npl-4* RNAi bacteria. Scale bar = 200 μm.

(C) Quantification of GFP levels of *sek-1(km4)* animals incubated on *P. aeruginosa*-GFP for 12 hours at 25°C after growth on the EV control, *ufd-1*, and *npl-4* RNAi bacteria. ***$P < 0.001$ via the *t*-test (n = 19–20 worms each).

(D) Representative survival plots of *sek-1(km4)* animals grown on bacteria for RNAi against *ufd-1* and *npl-4* along with the EV control at 20°C. Day 0 represents young adults. $P<0.001$ for *ufd-1* and *npl-4* RNAi compared to EV control.

(E) Representative survival plots of *dbl-1(nk3);pmk-1(km25)* animals on *P. aeruginosa* PA14 at 25°C after treatment with the EV control and *ufd-1* RNAi. $P<0.001$.

(F) Representative fluorescence images of *dbl-1(nk3);pmk-1(km25)* animals incubated on *P. aeruginosa*-GFP for 12 hours at 25°C after growth on the EV control and *ufd-1* RNAi bacteria. Scale bar = 200 μm.

(G) Quantification of GFP levels of *dbl-1(nk3);pmk-1(km25)* animals incubated on *P. aeruginosa*-GFP for 12 hours at 25°C after growth on the EV control and *ufd-1* RNAi bacteria. ***$P < 0.001$ via the *t*-test ($n = 24$ worms each).

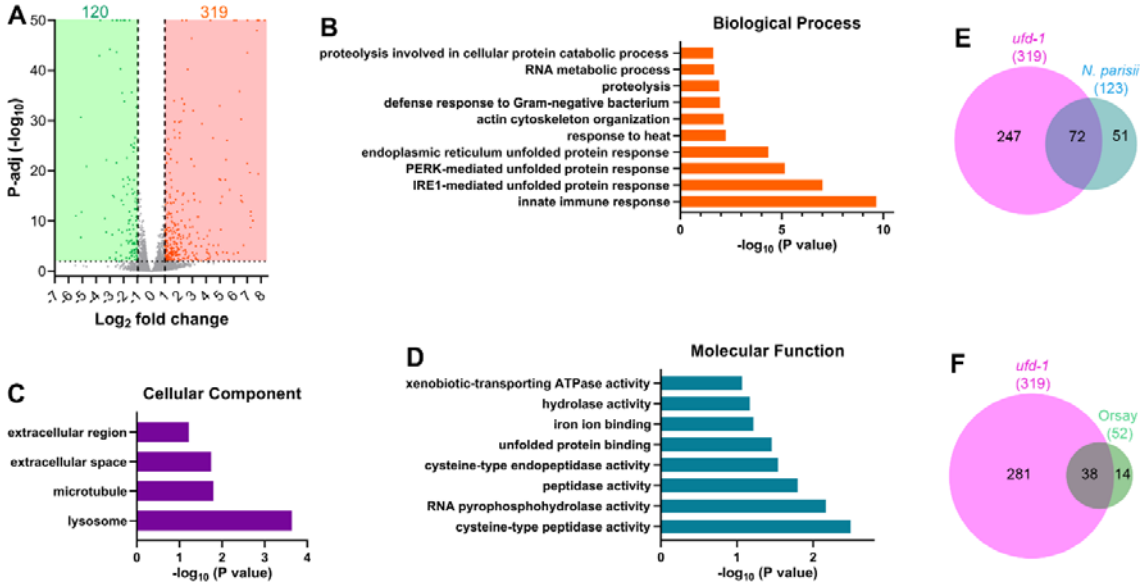

Figure 5. Knockdown of *ufd-1* results in the upregulation of protease and intracellular pathogen response genes

(A) Volcano plot of upregulated and downregulated genes in *ufd-1* RNAi versus empty vector (EV) control RNAi N2 animals. Orange and green dots represent significantly upregulated and downregulated genes, respectively, while the grey dots represent the genes that are not differentially regulated.

(B)-(D) Gene ontology enrichment analysis for *ufd-1* RNAi upregulated genes for biological processes (B), cellular component (C), and molecular function (D).

(E) Venn diagram showing the overlap between genes upregulated upon *ufd-1* RNAi and upregulated upon *Nematocida parisii* infection (Bakowski et al., 2014). The *P*-value for the overlap between the data is 8.2×10^{-110}.

(F) Venn diagram showing the overlap between genes upregulated upon *ufd-1* RNAi and upregulated upon Orsay virus infection (Sarkies et al., 2013). The *P*-value for the overlap between the data is 2.7×10^{-62}.

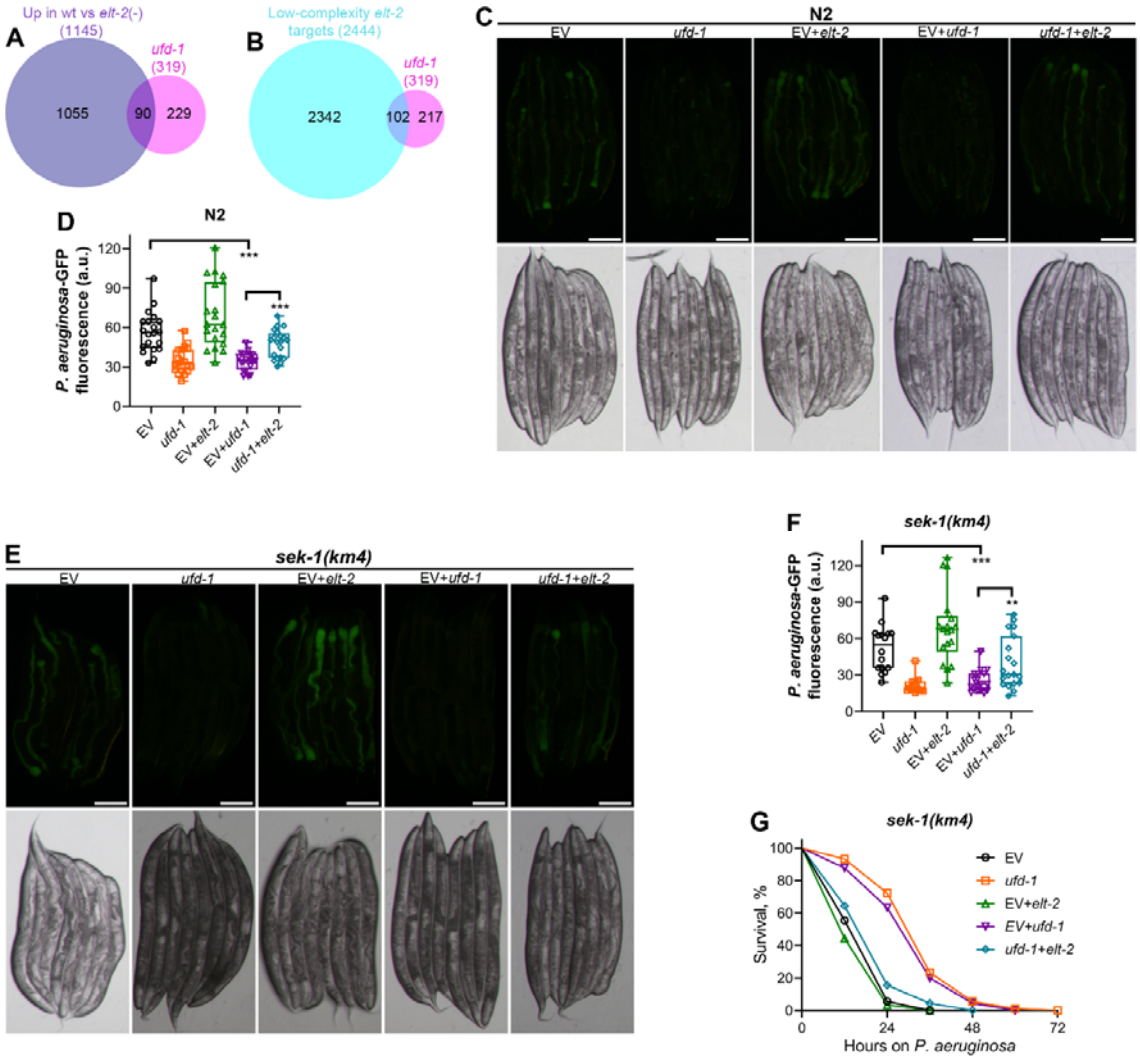

Figure 6. GATA transcription factor ELT-2 mediates the *ufd-1* knockdown phenotypes

(A) Venn diagram showing the overlap between genes upregulated upon *ufd-1* RNAi and upregulated in wt versus *elt-2*(-) larvae (Dineen et al., 2018). The *P*-value for the overlap between the data is 9.5×10^{-52}.

(B) Venn diagram showing the overlap between genes upregulated upon *ufd-1* RNAi and the low-complexity ELT-2 target genes (Mann et al., 2016). The *P*-value for the overlap between the data is 1.5×10^{-34}.

(C) Representative fluorescence (top) and the corresponding brightfield (bottom) images of N2 animals incubated on *P. aeruginosa*-GFP for 24 hours at 25°C after growth on the empty vector (EV) control, *ufd-1*, EV+*elt-2*, EV+*ufd-1*, and *ufd-1*+*elt-2* RNAi bacteria (see Methods for the details). Scale bar = 200 µm.

(D) Quantification of GFP levels of N2 animals incubated on *P. aeruginosa*-GFP for 24 hours at 25°C after growth on the EV control, *ufd-1*, EV+*elt-2*, EV+*ufd-1*, and *ufd-1+elt-2* RNAi bacteria. ***$P < 0.001$ via the *t*-test ($n = 20$ worms each).

(E) Representative fluorescence (top) and the corresponding brightfield (bottom) images of *sek-1(km4)* animals incubated on *P. aeruginosa*-GFP for 12 hours at 25°C after growth on the EV control, *ufd-1*, EV+*elt-2*, EV+*ufd-1*, and *ufd-1+elt-2* RNAi bacteria. Scale bar = 200 μm.

(F) Quantification of GFP levels of *sek-1(km4)* animals incubated on *P. aeruginosa*-GFP for 12 hours at 25°C after growth on the EV control, *ufd-1*, EV+*elt-2*, EV+*ufd-1*, and *ufd-1+elt-2* RNAi bacteria. ***$P < 0.001$ and **$P < 0.01$via the *t*-test ($n = 16$–19 worms each).

(G) Representative survival plots of *sek-1(km4)* animals on *P. aeruginosa* PA14 at 25°C after treatment with the EV control, *ufd-1*, EV+*elt-2*, EV+*ufd-1*, and *ufd-1+elt-2* RNAi bacteria. P<0.001 for *ufd-1+elt-2* RNAi compared to EV+*ufd-1* RNAi.

Supplementary Figures

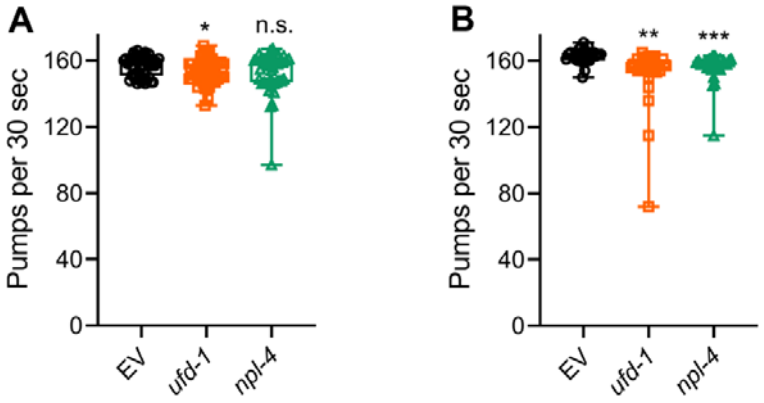

Figure S1. Inhibition of the UFD-1-NPL-4 complex does not affect the pharyngeal pumping rate

(A) Pharyngeal pumps per 30 sec of N2 animals grown on *ufd-1* and *npl-4* RNAi along with the empty vector (EV) control RNAi. $*P < 0.05$ via the *t*-test. n.s., nonsignificant ($n = 45$ worms each).

(B) Pharyngeal pumps per 30 sec of N2 animals grown on EV control, *ufd-1*, and *npl-4* RNAi followed by incubation on *P. aeruginosa* PA14 at 25°C for 12 hours. $***P < 0.001$ and $**P < 0.01$ via the *t*-test ($n = 30$ worms each).

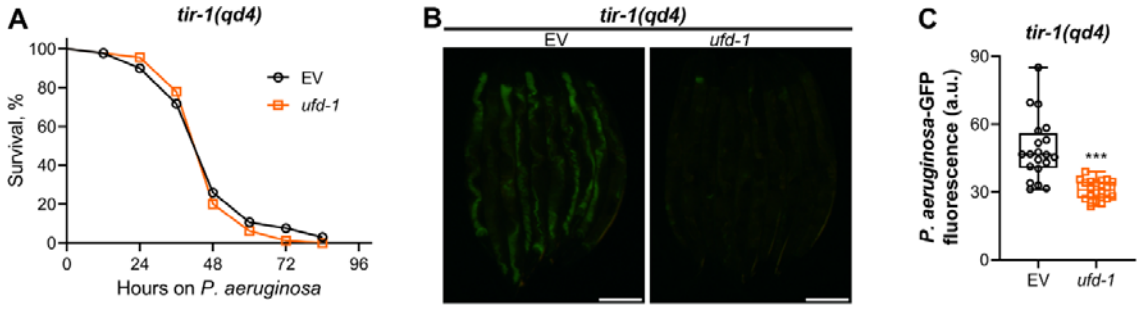

Figure S2. Reduced gut colonization upon *ufd-1* knockdown is independent of the *tir-1* immunity pathway

(A) Representative survival plots of *tir-1(qd4)* animals on *P. aeruginosa* PA14 at 25°C after treatment with the empty vector (EV) control and *ufd-1* RNAi. The difference between the EV and *ufd-1* RNAi survival plots is nonsignificant.

(B) Representative fluorescence images of *tir-1(qd4)* animals incubated on *P. aeruginosa*-GFP for 24 hours at 25°C after growth on the EV control and *ufd-1* RNAi bacteria. Scale bar = 200 μm.

(C) Quantification of GFP levels of *tir-1(qd4)* animals incubated on *P. aeruginosa*-GFP for 24 hours at 25°C after growth on the EV control and *ufd-1* RNAi bacteria. ***$P < 0.001$ via the *t*-test ($n = 20$ worms each).

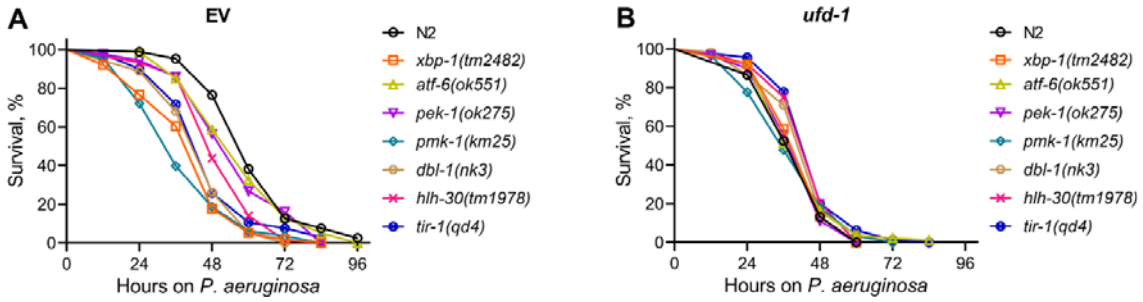

Figure S3. Knockdown of *ufd-1* dictates survival of different worm strains on *P. aeruginosa*

(A) Representative survival plots of worm strains on *P. aeruginosa* PA14 at 25°C after treatment with the empty vector (EV) control RNAi.

(B) Representative survival plots of worm strains on *P. aeruginosa* PA14 at 25°C after treatment with *ufd-1* RNAi.

The data in (A) and (B) is pooled from the data from Figures 1-3 and Figure S2.

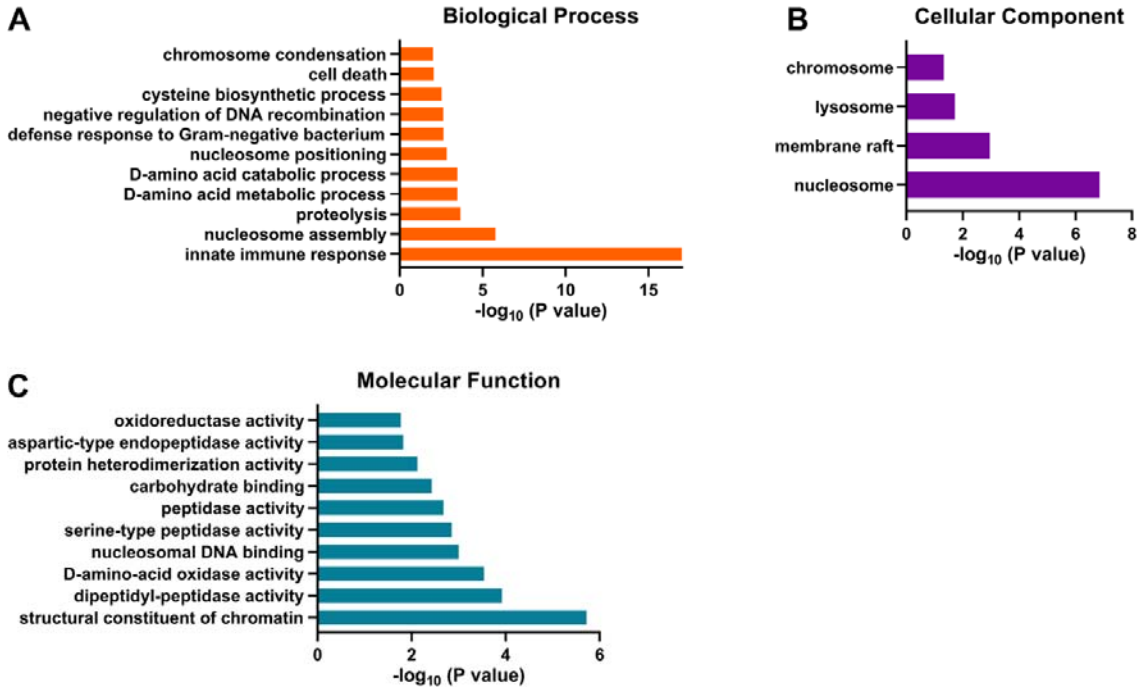

Figure S4. Gene ontology enrichment analysis for *ufd-1* RNAi downregulated genes

(A)-(C) Gene ontology enrichment analysis for *ufd-1* RNAi downregulated genes for biological processes (A), cellular component (B), and molecular function (C).

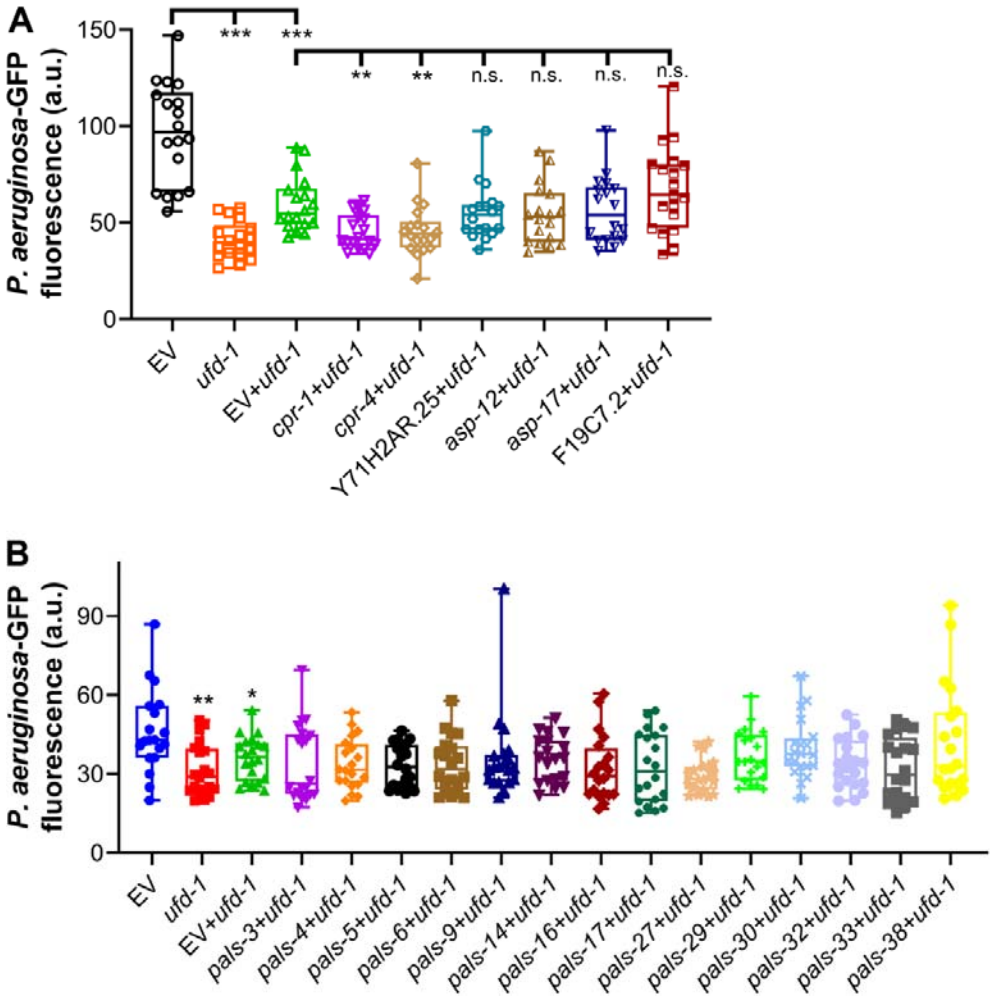

Figure S5. Individual protease or intracellular pathogen response genes are not involved in reduced colonization of *ufd-1* RNAi animals

(A) Quantification of GFP levels of N2 animals incubated on *P. aeruginosa*-GFP for 24 hours at 25°C after growth on indicated RNAi bacteria. *P*-values in comparison to EV and EV+*ufd-1* RNAi are indicated. ***$P < 0.001$ and **$P < 0.01$ via the *t*-test. n.s., nonsignificant ($n = 18$–19 worms each).

(B) Quantification of GFP levels of N2 animals incubated on *P. aeruginosa*-GFP for 24 hours at 25°C after growth on indicated RNAi bacteria. *P*-values in comparison to EV are shown. *P*-values for all the co-RNAi treatments in comparison to EV+*ufd-1* RNAi are nonsignificant. $n = 19$–20 worms each.

Table S1: Upregulated and downregulated genes in *ufd-1* RNAi versus empty vector (EV) control RNAi N2 animals. Genes exhibiting at least two-fold change and *P*-value <0.01 were considered differentially expressed.